JOURNAL OF THEORETICAL
AND APPLIED MECHANICS
https://doi.org/10.15632/jtam-pl/203600
ONLINE FIRST

FIELD PATH DETECTION FOR TRACTORS BASED ON ACCELERATION MEASUREMENTS AND MULTIBODY SYSTEM SIMULATIONS

Wilhelm FUCHS[1], Gernot JEDINGER-PAUSCHENWEIN[1], Helmut J. HOLL[2*]

[1] *AVL List GmbH, Tech-Center Steyr, Austria*
[2] *Institute of Technical Mechanics, Johannes Kepler University, Linz, Austria*
*corresponding author, *helmut.holl@jku.at*

A process is described that allows the identification of the road profile traversed by a tractor based only on acceleration signals measured in the field. The objective of this identification process is to obtain a field path profile that, when simulated, produces accelerations in the tractor as close as possible to those generated by the original profile, thereby causing similar damage values to the structure of the tractor. This process requires an accurate multibody system model of the vehicle with a sophisticated tire model. Under these considerations a method has been developed making it possible to invert the dynamic problem and to determine the field path profile, which can subsequently be used for simulations of arbitrary tractors.

Keywords: vehicle; multibody system; Adams; inverse dynamics; identification.

1. Introduction

Virtual development of tractors requires an accurate load case definition with a reasonable correspondence between simulation and real-world field conditions, which is the fundamental prerequisite for the strength and mechanical fatigue analysis (see (Renius, 2020)). The predominantly used input load parameters are the forces at the wheel hubs and excitations caused by the field path profile.

A well-established method to measure the forces at the wheel hubs is to use measurement rims (see Fig. 1), although this approach is time consuming (Ferhadbegović, 2008).

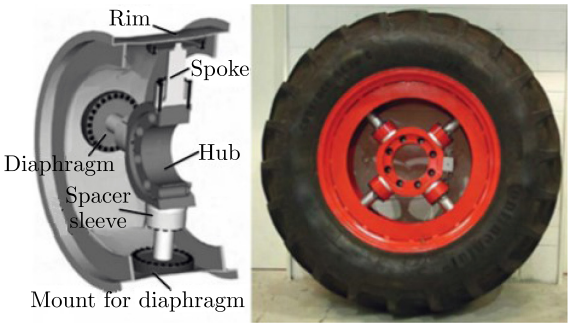

Fig. 1. Measurement rim.

Ministry of Science and Higher Education
Republic of Poland

The publication has been funded by the Polish Ministry of Science and Higher Education under the Excellent Science II programme "Support for scientific conferences".
The content of this article was presented during the 40th Danubia-Adria Symposium on Advances in Experimental Mechanics, Gdańsk, Poland, September 24–27, 2024.

Moreover, these forces are specific to one particular parameter set, whereby even a minor change (e.g., adjusting ballast mass, using another implement, etc.) makes these measured forces unusable for further simulations with the established tractor model.

Therefore, parameters are needed which are independent of the specific tractor configuration. Since the field path profile fulfills this requirement, it emerges as a promising approach (also see (Gattringer, 2023)).

2. Field path detection based on measured accelerations

An accurate multibody system simulation model of the tractor including a high sophisticated tire model is the prerequisite for field path detection, which has been elaborated in (Fuchs & Pauschenwein, 2019; Jedinger-Pauschenwein *et al.*, 2024).

For setting up the multibody system (see (Schrattbauer, 2024)), the software system Adams, version 2022.2.0, has been used in combination with FTire. Adams is a multibody dynamics simulation software system (see (Adams)), whereas FTire is used for modeling tires (see (Gipser, 2007; Leister, 2009; Oertel, 2007; FTire)).

The method presented here allows the identification of the road profile traversed by a tractor based solely on measuring accelerations.

The target is to derive a profile that, when simulated, generates accelerations in the tractor as closely as possible to those generated by the original profile. As a result, the identification of the road profile excitations on basis of measured accelerations is an inverse problem.

Considering an inverse problem, a simplified model with a reduced number of degrees of freedom seems to be advantageous. Therefore, such a model is derived from the complex nonlinear tractor model in Adams replicating the dynamic behavior of the real tractor very accurately. Referring to Schiller (2018) comparative simulations proved that a reasonable reduction of degrees of freedoms has a negligible influence on the accelerations (e.g., fixing cabin rigidly to the tractor body, etc.). Furthermore, the high sophisticated FTire model is replaced by a spring damper system, and further simplifications of the inverse problem are achieved by linearization.

2.1. Mathematical framework

Linear time-invariant mechanical systems are characterized by the differential equation:

$$\mathbf{M}\ddot{\mathbf{s}} + \mathbf{D}\dot{\mathbf{s}} + \mathbf{K}\mathbf{s} = \mathbf{f}. \tag{2.1}$$

Description of the parameters and the variables:

q	–	number of degrees of freedom,	$\mathbf{M} \in \mathbb{R}^q \times \mathbb{R}^q$	–	mass matrix,
$\mathbf{s} \in \mathbb{R}^q$	–	generalized displacement vector,	$\mathbf{D} \in \mathbb{R}^q \times \mathbb{R}^q$	–	damping matrix,
$\dot{\mathbf{s}} \in \mathbb{R}^q$	–	generalized velocity vector,	$\mathbf{K} \in \mathbb{R}^q \times \mathbb{R}^q$	–	stiffness matrix,
$\ddot{\mathbf{s}} \in \mathbb{R}^q$	–	generalized acceleration vector,	$\mathbf{f} \in \mathbb{R}^q$	–	external forces vector.

Using the substitution $\dot{\mathbf{s}} = \mathbf{v}$ and adjusting the notation such that $\mathbf{M}^{-1}\mathbf{f} = \widehat{\mathbf{B}}\mathbf{u}$ leads to a first order system of linear differential equations:

$$\begin{bmatrix} \dot{\mathbf{s}} \\ \dot{\mathbf{v}} \end{bmatrix} = \underbrace{\begin{bmatrix} \mathbf{0} & \mathbf{E} \\ -\mathbf{M}^{-1}\mathbf{K} & -\mathbf{M}^{-1}\mathbf{D} \end{bmatrix}}_{\mathbf{A}} \begin{bmatrix} \mathbf{s} \\ \mathbf{v} \end{bmatrix} + \underbrace{\begin{bmatrix} \mathbf{0} \\ \widehat{\mathbf{B}} \end{bmatrix}}_{\mathbf{B}} \mathbf{u}. \tag{2.2}$$

Introducing the state vector $\mathbf{x}^{\mathrm{T}} = \left[\mathbf{s}^{\mathrm{T}}, \mathbf{v}^{\mathrm{T}}\right]$, the linear time-invariant (LTI) system results in a more compact form, whereby the wheel hub forces are collected in the input vector $\mathbf{u}$:

$$\dot{\mathbf{x}} = \mathbf{A}\mathbf{x} + \mathbf{B}\mathbf{u} \quad \text{with} \quad \mathbf{y} = \mathbf{C}\mathbf{x} + \mathbf{D}_T\mathbf{u}. \tag{2.3}$$

Description of the matrices

$\mathbf{A} \in \mathbb{R}^n \times \mathbb{R}^n$	– system matrix	$\mathbf{C} \in \mathbb{R}^k \times \mathbb{R}^n$	– output matrix
$\mathbf{B} \in \mathbb{R}^n \times \mathbb{R}^m$	– input matrix	$\mathbf{D}_T \in \mathbb{R}^k \times \mathbb{R}^m$	– direct transmission matrix.

This LTI system comprises matrices $\mathbf{A}$, $\mathbf{B}$, $\mathbf{C}$, $\mathbf{D}_T$, state vector $\mathbf{x} \in \mathbb{R}^n$ (positions and velocities), input vector $\mathbf{u} \in \mathbb{R}^m$, and output vector $\mathbf{y} \in \mathbb{R}^k$.

Since in this study the direct transmission matrix $\mathbf{D}_T$, not to be confused with the damping matrix $\mathbf{D}$, is consistently zero, the output vector (measured variables) can be expressed as

$$\mathbf{y} = \mathbf{C}\mathbf{x}. \tag{2.4}$$

Differentiating Eq. (2.4) and substituting the vector $\dot{\mathbf{x}}$ from Eq. (2.3), $\dot{\mathbf{y}}$ becomes

$$\dot{\mathbf{y}} = \mathbf{C}\mathbf{A}\mathbf{x} + \mathbf{C}\mathbf{B}\mathbf{u}. \tag{2.5}$$

Reorganizing the terms to isolate the input vector $\mathbf{u}$ leads to

$$\mathbf{u} = (\mathbf{C}\mathbf{B})^{-1} \cdot \left[\dot{\mathbf{y}} - \mathbf{C}\mathbf{A}\mathbf{C}^{-1}\mathbf{y}\right]. \tag{2.6}$$

Generally, matrix $\mathbf{C}$ possesses dimensions $k \times n$ while matrix $\mathbf{B}$ has $n \times m$. Upon multiplying these matrices, the resulting dimensions of $\mathbf{CB}$ are $k \times m$. If m is equal to k, and assuming $\mathbf{CB}$ is regular, it could be conventionally inverted. However, for non-square $\mathbf{CB}$ matrices, the equation has to be modified to (see (Freund & Hoppe, 2007)):

$$\mathbf{u} = (\mathbf{C}\mathbf{B})^{+} \cdot \left[\dot{\mathbf{y}} - \mathbf{C}\mathbf{A}\mathbf{C}^{-1}\mathbf{y}\right], \tag{2.7}$$

with the so-called Moore–Penrose pseudo-inverse for non-square matrices $\mathbf{CB}$, which is described in (Freund & Hoppe, 2007):

$$(\mathbf{C}\mathbf{B})^{+} = \left[\mathbf{B}^{\mathrm{T}}\mathbf{C}^{\mathrm{T}}\mathbf{C}\mathbf{B}\right]^{-1}\mathbf{B}^{\mathrm{T}}\mathbf{C}^{\mathrm{T}}. \tag{2.8}$$

Using the abbreviation $\mathbf{S} = \mathbf{B}^{\mathrm{T}}\mathbf{C}^{\mathrm{T}}\mathbf{C}\mathbf{B}$, the pseudo-inverse becomes

$$(\mathbf{C}\mathbf{B})^{+} = \mathbf{S}^{-1}\mathbf{B}^{\mathrm{T}}\mathbf{C}^{\mathrm{T}}, \tag{2.9}$$

and Eq. (2.7) transforms to

$$\mathbf{u} = \mathbf{S}^{-1}\mathbf{B}^{\mathrm{T}}\mathbf{C}^{\mathrm{T}} \cdot \left[\dot{\mathbf{y}} - \mathbf{C}\mathbf{A}\mathbf{C}^{-1}\mathbf{y}\right]. \tag{2.10}$$

Matrix $\mathbf{S}$ must be invertible for this algorithm's application. This necessitates matrix $\mathbf{C}$ to be regular. Considering this relationship, the input variables of an LTI-system can be deduced, and this research indicates that, in general, the addressed problem is a pseudo-inverse one.

A significant merit of this approach is the elimination of frequency domain transformations which are normally used for inversion by virtual iteration (see (Gattringer, 2023; Reichl, 2011; Witteveen, 2023)). Furthermore, matrix $\mathbf{S}$ requires only one single inversion, regardless of the computed time steps, as it comprises fixed values.

Since the second derivation of the positions is measurable (accelerations), only signal integration is required to obtain $\dot{\mathbf{y}}$ and $\mathbf{y}$, which is a stable numerical procedure. In this special case it has been chosen for simplicity without loss of generality that $\dot{\mathbf{y}} = \dot{\mathbf{x}}$ and $\mathbf{y} = \mathbf{x}$.

Knowing the forces $\mathbf{u}$, the state vector $\mathbf{x}$, tire stiffness and damping, a differential equation is applied to deduce the field path profile (ground elevation $\mathbf{x}_G$) considering the geometry referring to the tire radius.

2.2. Identification of wheel center point displacement

The system description (2.2) and (2.3), along with its inverted variant (2.10), is relevant only for systems that have forces as their inputs, but field path detection requires a further relation between forces and displacements which will be the final inputs.

To establish the relationship between force and displacement, a single-mass oscillator composed of a spring and damper is utilized, as depicted in Fig. 2. In this context, the linear spring/damper model approximates the complex stiffness and damping properties of the tire. Consequently, the values for the spring constant k and the damping coefficient d can be derived from parameters of the FTire-model.

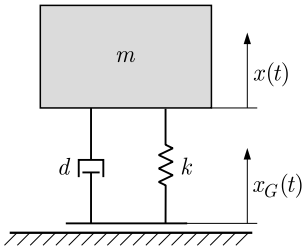

Fig. 2. One-mass-oscillator.

The equation of motion for the mass in Fig. 2 is

$$m\ddot{x} = -d(\dot{x}_G - \dot{x}) - c(x_G - x), \tag{2.11}$$

where x and $\dot{x}$ represent the vertical position and velocity of the wheel center point (WCP). Both state variables are obtained from the simulation directly or from integration of the sensor signal. The force F, which is identical to the right side of Eq. (2.11), has been determined by the inverse algorithm to identify the wheel hub forces. As a result, it becomes feasible to determine x_G by solving the differential equation:

$$\dot{x}_G = \frac{c(x - x_G) + d\dot{x} + F}{d}. \tag{2.12}$$

In simulations with different profiles, it is not ensured that, even with otherwise unchanged simulation parameters, the average speed remains the same. This implies that when comparing two simulation results over the time parameter, a reliable comparability of the state variables cannot be guaranteed.

However, as part of the iteration process, it is essential to compare and link state variables from different simulations with varying track profiles. For the before mentioned reason, the dependence on time is transformed into a dependence on distance $s(t)$. By introducing

$$v(t) = \frac{\mathrm{d}s(t)}{\mathrm{d}t} \tag{2.13}$$

and applying the chain rule

$$\frac{\mathrm{d}x(s(t))}{\mathrm{d}t} = \frac{\mathrm{d}x(s(t))}{\mathrm{d}s} v(t) \rightarrow \frac{\mathrm{d}x(s)}{\mathrm{d}s} = \frac{\mathrm{d}x(t)}{\mathrm{d}t} \frac{1}{v(t)}. \tag{2.14}$$

Equation (2.12) results in

$$\frac{\mathrm{d}x_G(s)}{\mathrm{d}s} = \frac{c(x(s) - x_G(s)) + d\dot{x}(s) + F(s)}{d} \frac{1}{v(s)}. \tag{2.15}$$

To transform the simulation data from the time domain to the space domain, the variable x_{td} (traveled distance) was introduced. This variable integrates the longitudinal velocity component

of the chassis center of mass, storing the distance covered at each sample time point (the traveled distances of the wheel hub centers should be identical with x_{td} of the chassis center of mass). By replacing the time vector with the resulting displacement vector, the state variable data can be transformed into the space domain.

Generally, it is important to realize that traversing a road profile in reality involves a tire with a non-zero radius, as sketched in Fig. 3.

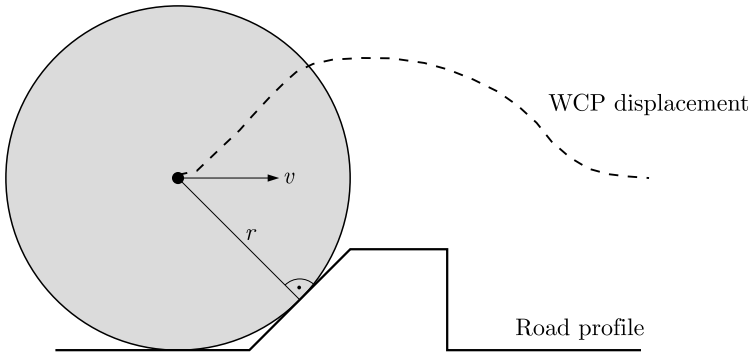

Fig. 3. Merry-go-round profile.

The line connecting the point of contact to the wheel center is supposed to remain always approximately normal to the road profile. This implies that the resulting movement of the wheel center will not represent the geometry of the traversed profile. Therefore, it becomes essential to construct the road profile from the determined displacements of the wheel center points.

Moreover, it is crucial to recognize that the determination of wheel center point movements, based on the differential Eq. (2.2), presupposes that the tire's contact with the road occurs precisely at a single point vertically below the wheel center point. However, this is an idealized simplification, because multi-point contacts as illustrated in Fig. 3 can occur as well as tire's compression at edges (see Fig. 4). Due to these multi-point contacts and extreme tire deflections the field path profile cannot be captured accurately within this section.

Fig. 4. Tire compressed by edge.

Regarding the influence of tire radii on the quality of identification, this study aims to demonstrate that an identified profile achieves satisfactory accelerations even when traversed with tires of larger radii. As a result, re-identification is not necessary when using tires with larger radii.

Another point to consider is that during the simulation or during the field test, one or more wheels may lift off the roadway. It is impossible for the identification algorithm to distinguish between an actual lift off and a touching road profile. In addition, tires starting to skid can cause another problem: since the identified profiles will always differ from the original profile, these effects will never occur at the same time, with the same duration, or at the same place in subsequent simulations of an iteration.

As a result, there can be phase shifts in the acceleration signals of different simulations. All these real-world effects influence the identified road profile, whereby a geometrically precise identification of the road profile using this method seems to be unattainable.

For future investigations it may be expected that AI-methods incorporate potential for further improvements concerning the identification and inversion process.

Nevertheless, it must be emphasized that the highest accuracy is not the primary aim, anyway. The goal is to ensure that the accelerations resulting from the identified road profile sufficiently approximate the accelerations caused by the original road profile, because in this case the damage values referring to the identified road profile can be expected satisfactorily close related to those caused by the original road profile, see (Fuchs *et al.*, 2024).

2.3. Road generation

The unknown track profile can be generated from the identified wheel center point deflections using geometrical considerations. As already explained in the preceding section, the wheel center point deflections arise approximately by following the line always perpendicular to the track with a length of the constant tire radius r as illustrated in Fig. 3.

The track profile can now be determined in the opposite manner. The derivative of the wheel center point deflection p_{WCP} defines $g(s)$ as

$$\frac{\mathrm{d}p_{\mathrm{WCP}}(s)}{\mathrm{d}x} = g(s), \tag{2.16}$$

and the gradient of the deflection curve is

$$\mathbf{g}(s) = \begin{pmatrix} 1 \\ g(s) \end{pmatrix}. \tag{2.17}$$

By rotating the gradient by 90° clockwise, one obtains

$$\acute{\mathbf{g}}(s) = \begin{pmatrix} g(s) \\ -1 \end{pmatrix}. \tag{2.18}$$

As a unit vector multiplied by the tire radius r_W, the desired vector

$$\mathbf{g}_r(s) = \frac{1}{|\acute{\mathbf{g}}(s)|}\acute{\mathbf{g}}(s) r_W \tag{2.19}$$

is obtained, pointing from the current wheel center point position to the corresponding contact point or point on the track. Adding the wheel center point position and the vector (Eq. 2.19) yields the absolute position of the current track point.

Adding the tire radius in the z-direction (vertical) ensures that the track coordinate in the z-direction starts at 0:

$$\mathbf{p}_R(s) = \mathbf{p}_{\mathrm{WCP}}(s) + \mathbf{g}_r(s) + \begin{pmatrix} 0 \\ r_W \end{pmatrix}. \tag{2.20}$$

Since the longitudinal components of the tire contact forces are known from the Adams simulation, and the longitudinal stiffnesses k_{Long} of the tires are available, the determined position of the current contact point can be further corrected in the x-direction by estimating

$$c(s) = \frac{F_{\mathrm{Long}}(s)}{k_{\mathrm{Long}}(s)} \tag{2.21}$$

as an additional shift:

$$\mathbf{p}(s) = \mathbf{p}_{\mathrm{WCP}}(s) + \mathbf{g}_r(s) + \begin{pmatrix} c(s) \\ r_W \end{pmatrix}. \tag{2.22}$$

A significant observation is that the road created using this method cannot generally be directly utilized. This stems from the fact that it cannot be assumed that in the identified wheel center point movements, all local radii of curvature are greater than or equal to the idealized tire radius as already mentioned (see Fig. 4).

If the radii of curvature are smaller than the tire radius, a track profile can emerge that self-penetrates, resulting in road points whose x-coordinates have multiple z-coordinates.

This phenomenon is illustrated in Fig. 5, which exemplifies such a generated road.

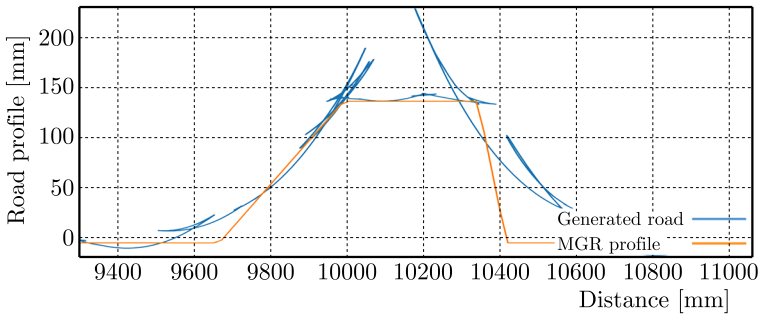

Fig. 5. Generated road profile from identified wheel center point movements.

Realistically, such tracks cannot be either created or traversed. Addressing these issues requires additional considerations. A sorting of all the generated track points according to their x-coordinates has been conducted. This sorting ensures a track with a unique x/z mapping. Figure 6 displays the track that results from sorting the track shown in Fig. 5.

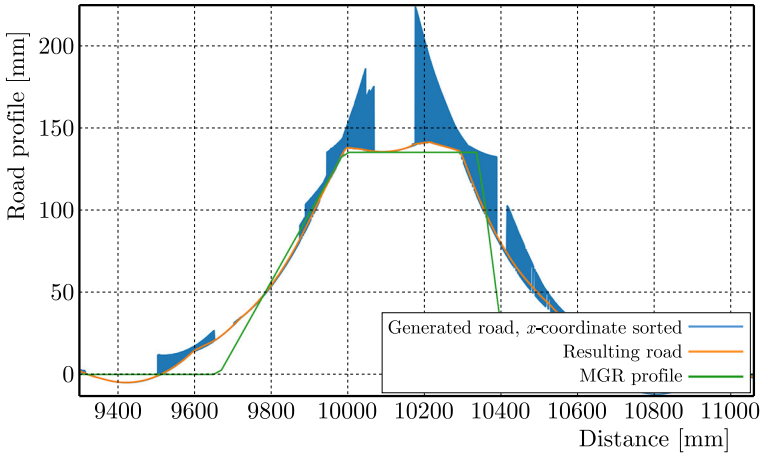

Fig. 6. Generated road profile with sorted x-coordinates.

Having achieved a unique x/z mapping, the next step involves eliminating the peaks that arose during the sorting process. This elimination is executed via a search algorithm. Starting from the current point, the algorithm searches for the first point in the x-direction such that the connecting line between the points does not exceed a predetermined maximum gradient value.

This newly identified point then serves as the starting point for subsequent searches. The final profile generated through this process is depicted in Fig. 6. This methodical approach ensures a road profile that can be used in subsequent simulations.

A summarizing description of the identification algorithm is described in Fig. 7.

The original accelerations refer to a complex nonlinear model, especially in view of the highly sophisticated tire model. Since identifications are carried out with the simplified LTI models, the identified profiles deviate from the original one. Therefore, a virtual iteration process in the time domain has been developed so that the identified solutions should converge to the original profiles (see Fig. 8).

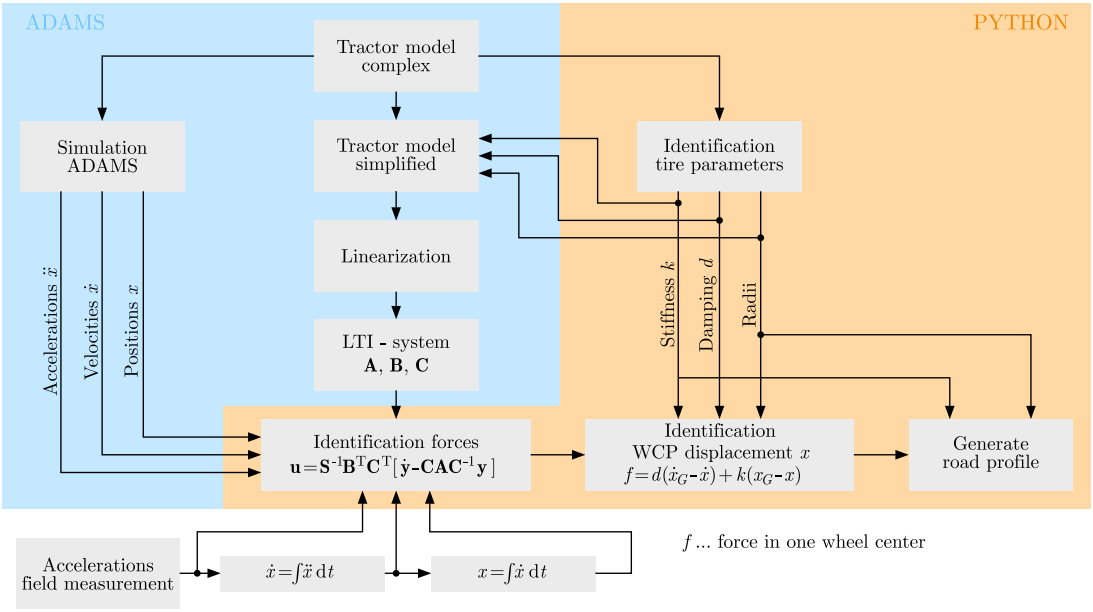

Fig. 7. Identification algorithm.

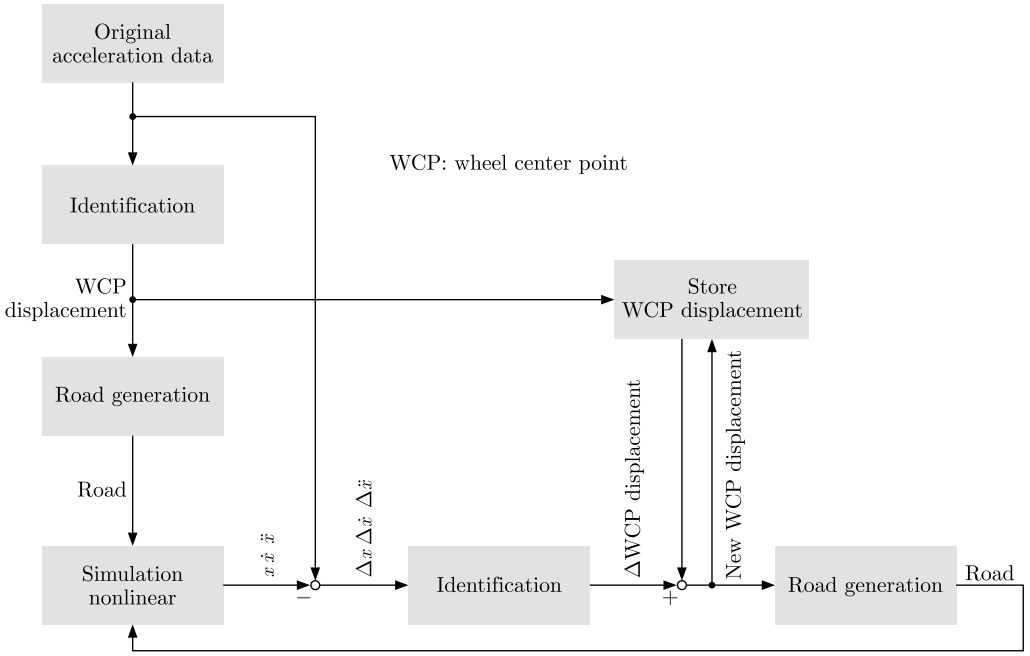

Fig. 8. Iteration process for road identification.

However, it must be emphasized that convergence cannot be warranted, and it has to be checked with a keen eye whether the process is successful and whether the iterated accelerations are sufficiently close to the original ones.

2.4. Simplified model for inversion

It is crucial to select an appropriate number of degrees of freedom and, consequently, an adequate number of state variables (see (Popp & Schiehlen, 2010; Shabana, 2013)). Typically, a rigid body possesses six degrees of freedom, encompassing movements in the x-, y-, and z-directions, and rotations about these axes. An additional degree of freedom arises from the front axle, which can rotate about the longitudinal axis independently of the main chassis in the case presented here.

In the context of the simplified model, movement in the longitudinal direction is not considered, and the model is fixed in this direction at the center of gravity. Additionally, the movement of the center of gravity in the lateral direction and its rotation about the vertical axes have been selected as the fifth and sixth degrees of freedom.

Consequently, the following six degrees of freedom remain:

1) movement of chassis in vertical direction;
2) movement of chassis in lateral direction;
3) rotation of chassis about vertical axis;
4) rotation of chassis about longitudinal axis;
5) rotation of chassis about lateral axis;
6) rotation of front axle about longitudinal axis of chassis.

These six degrees of freedom can be expressed via transformations of the six state variables (X_1, X_2, X_3, X_4, X_5, X_6), as seen in Fig. 9, where also the chosen combination of state variables and boundary conditions is illustrated.

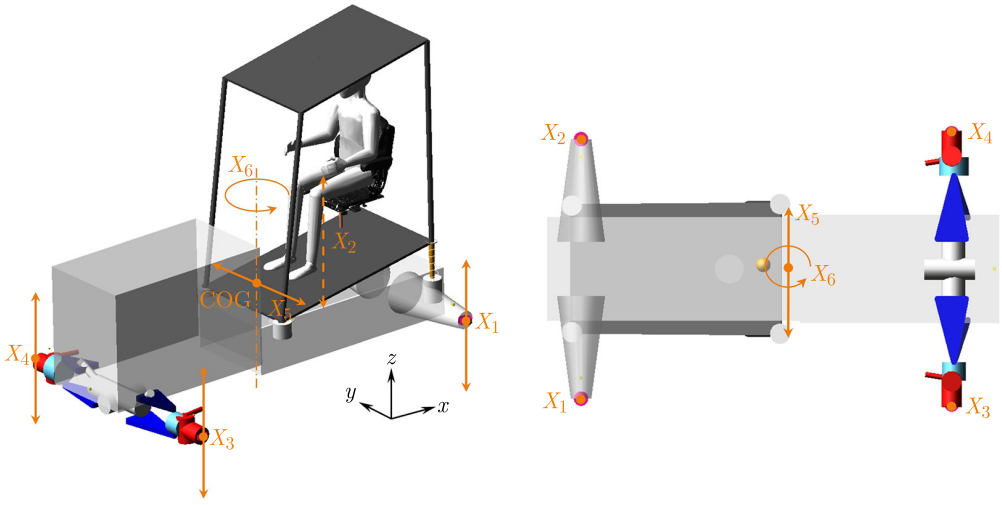

Fig. 9. Simplified model, state and boundary condition.

The four sensor locations from the nonlinear model, depicted in Fig. 10, are selected, whereby all sensors can measure accelerations in x-, y-, and z-directions. Without loss of generality, the sensor positions have been virtually shifted to the wheel center points, which requires transformations of the measured acceleration signals.

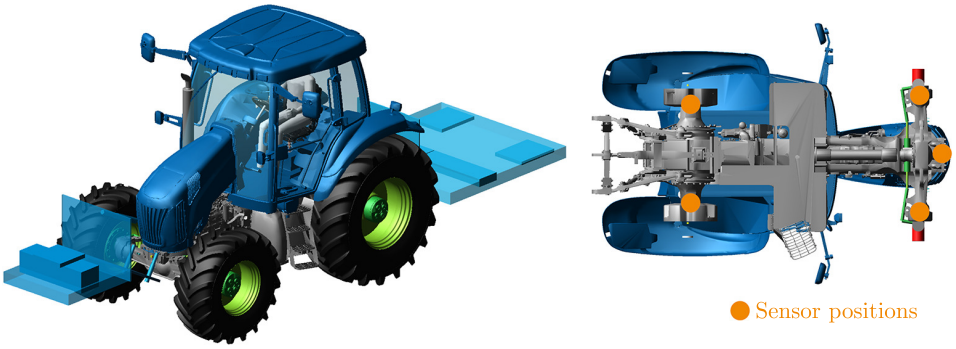

Fig. 10. Tractor, position of acceleration sensors.

All these transformations serve to reduce potential error sources during development, as the movement of the wheel center points is integral to the identification process.

Fortunately, this system comprises six degrees of freedom and six input parameters which are four vertical and two lateral forces (one lateral force per axle). As a result, in this case a direct inversion of the matrix **CB** is possible. If a swing arm at the front axle is to be considered, the number of degrees of freedom will be greater than the number of input parameters, which requires the application of the Moore-Penrose pseudo-inversion.

3. Examples for field path detection

General remark: references to measurement details (tractor manufacturer, test location) cannot be provided because of confidentiality agreements with AVL's customer.

3.1. Merry-go-round test

The merry-go-round test (MGR) is specifically designed to test the durability and resilience of vehicles when exposed to real or simulated working conditions, whereby periodical excitations due to obstacles as shown in Figs. 11 and 12 are to be considered. In literature it is also referred to as a bump test track circuit with obstacles (see (Renius, 2020)).

Fig. 11. Merry-go-round test.

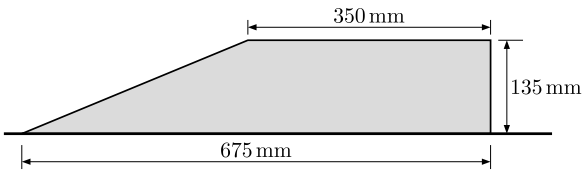

Fig. 12. Obstacle in detail.

A tractor was tested with a speed of 7.5 km/h. Based on accelerations measured close to the wheel hub centers, the obstacle shape has been identified, as seen in Fig. 13.

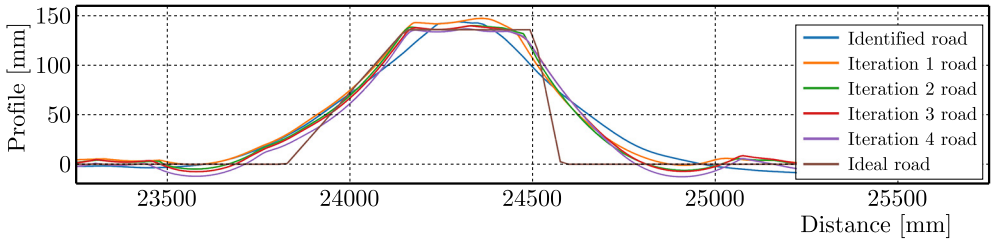

Fig. 13. MGR, 7.5 km/h, path profile.

However, the comparison between Figs. 12 and 13 indicates that the iterated profile does not match the original one exactly. The reason for the deviations can be explained by the following example.

For simplicity, a stiff disc is considered instead of an elastic tire, and furthermore, it is assumed that there will be no loss of contact between the profile and the disc. Even with these extremely simplified conditions it gets obvious that the red profile in Fig. 14 will cause the same vertical wheel center movement as the original black one, which means that in some cases the road profile cannot be uniquely determined on the basis of acceleration measurements.

In reality contact loss and multi-point contacts can additionally occur as well as compression of the tires at edges (see Fig. 4). It is impossible for the identification algorithm to distinguish between an actual lift off and a slight touching of the road profile. This is an illustrative explanation that convergence cannot be warranted. Therefore, it always must be checked if the iterated accelerations are sufficiently close to the original ones.

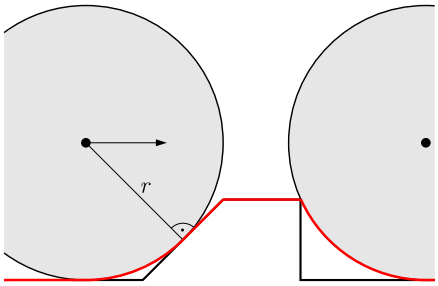

Fig. 14. Different road profiles achieving the same acceleration at wheel center point.

Nevertheless, Figs. 15 and 16 indicate that the acceleration results achieved with the identified profile correspond very well with the acceleration achieved with the original one. This is the most important condition for the simulation to present a realistic dynamic behavior of the tractor, also in view of subsequent strength and mechanical fatigue analyses.

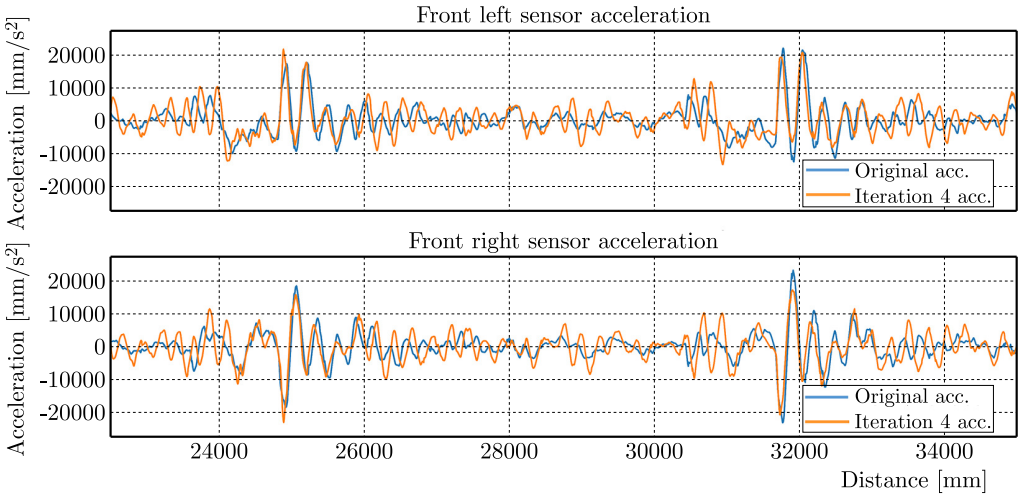

Fig. 15. MGR, 7.5 km/h, front acceleration.

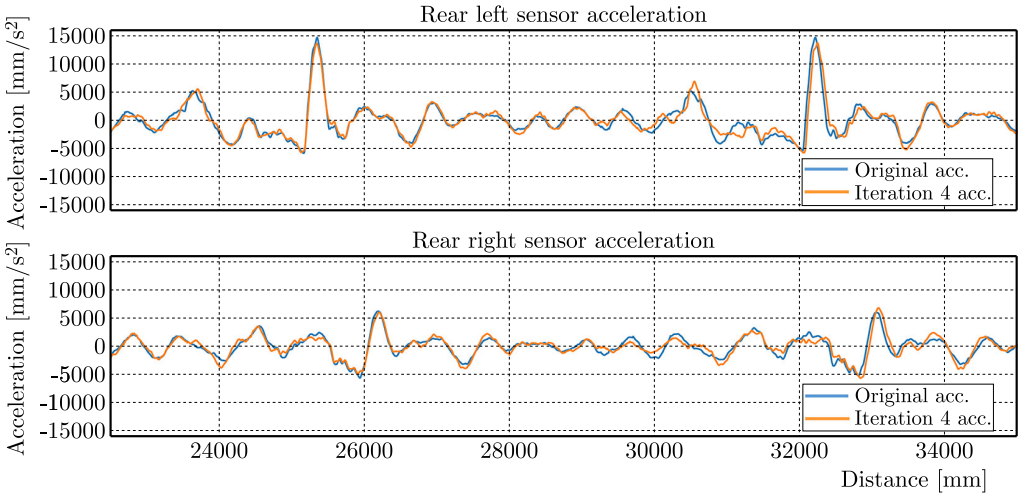

Fig. 16. MGR, 7.5 km/h, rear acceleration.

3.2. ISO 5008 track

The second test track was modeled on the basis of the ISO 5008 rougher road course (see (Wiesebrock, 2016)), the so-called Holperbahn-35 (jolting path or "Sturzacker") as seen in Fig. 17.

Fig. 17. ISO 5008, rougher road course in reality.

This road course was traversed unballasted at a speed of 7.5 km/h.

Although the ISO 5008 profile challenges the inversion algorithm with its instances of multiple-point tire contacts and several sharp edges, Fig. 18 indicates that the original and the identified field path profiles correspond very well.

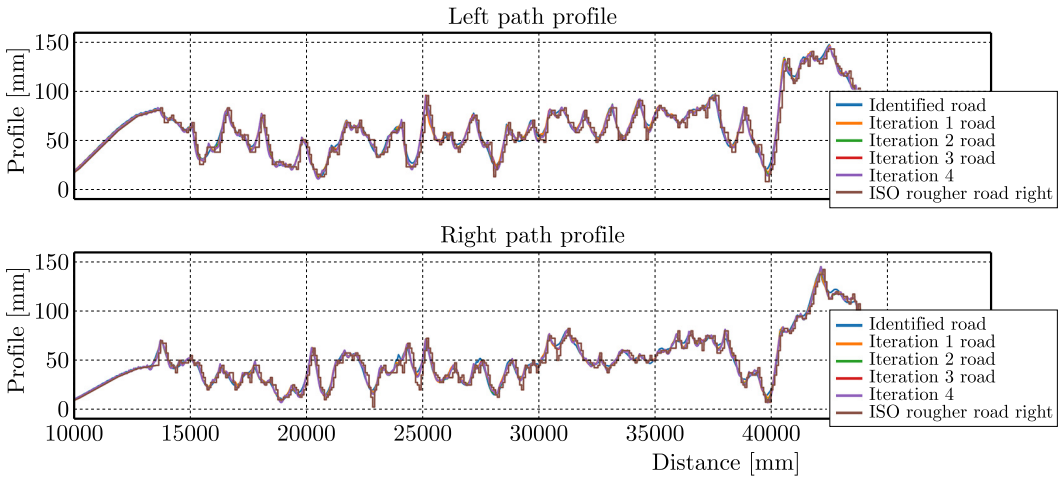

Fig. 18. ISO 5008, rougher road, path profile.

Nevertheless, a geometric match is not the ultimate objective, because the goal is to achieve vertical accelerations when traversing, which closely resemble the original ones. This must be verified by conducting another simulation using the identified track, and as seen in Figs. 19 and 20, the accelerations correspond sufficiently accurately with those achieved with the original profile, so that a satisfactory lifetime prediction should be possible.

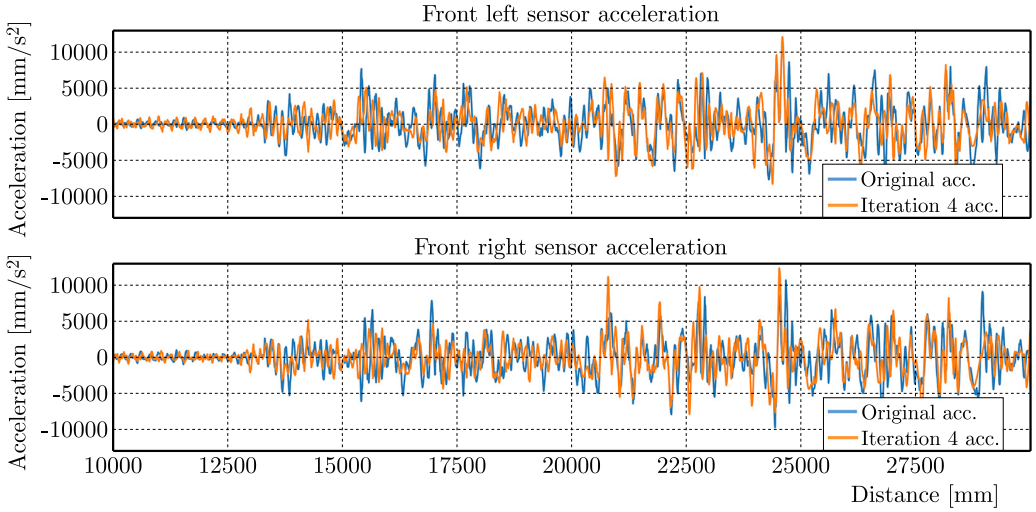

Fig. 19. ISO 5008, rougher road, 7.5 km/h, unballasted, front acceleration.

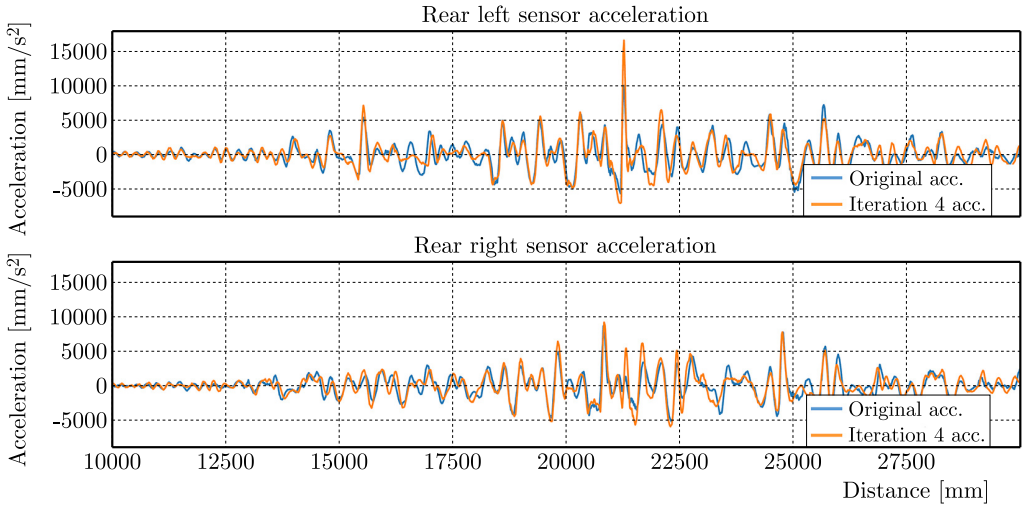

Fig. 20. ISO 5008, rougher road, 7.5 km/h, unballasted, rear acceleration.

3.3. Four-poster test rig

The four-poster test rig is designed to simulate working conditions in the field. It consists of four hydraulic actuators, each positioned under a wheel of the vehicle (see also (Reichl, 2011)). The objective is to achieve the same vertical accelerations as measured in the field. The presented inversion algorithm provides the input signals for the actuators, also for random and long test tracks. The simplified model is adjusted to the boundary conditions at the test bed, which means that the lateral degree of freedom is fixed by two bars at one front/rear wheel, as shown in Fig. 21. This measure and the fact that multiple tire contact surfaces cannot occur at the four-poster test rig accelerate the convergence.

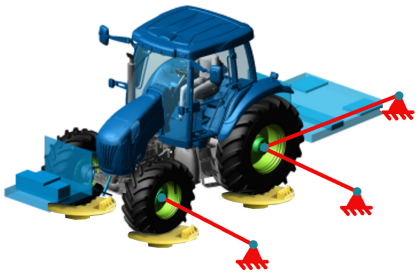

Fig. 21. Boundary conditions at four poster test rig.

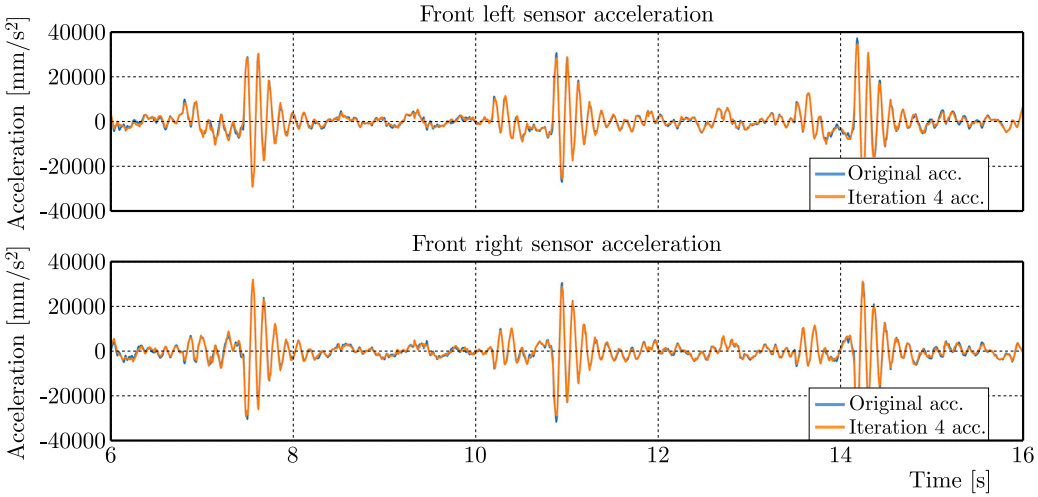

Fig. 22. Four-poster, MGR, 7.5 km/h, ballasted, front acceleration.

Using the merry-go-round test as example, Figs. 22 and 23 indicate that the target of reproducing the original acceleration on the test rig is met very well.

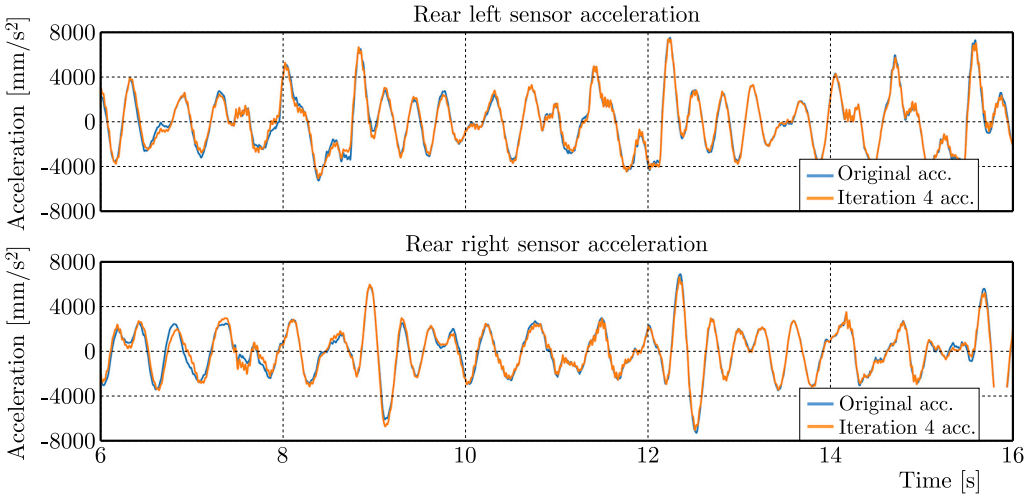

Fig. 23. Four-poster, MGR, 7.5 km/h, ballasted, rear acceleration.

4. Conclusions

An iterative method in the time domain has been established for field path detection based on measured accelerations. This method is cost-effective and sufficiently accurate as can be seen in the examples carried out.

Furthermore, in contrast to wheel hub forces, field path profiles do not depend on a certain set of tractor parameters, and therefore, they are outstandingly suitable for setting up an input data base for tractor multibody system simulations, also in view of different countries and farmlands.

Based on reliable input data, these tractor multibody system simulations will deliver sufficiently accurate load cases for the finite element analysis and mechanical fatigue life prediction, which is a prerequisite for the weight optimized tractor design.

For the future it may be expected that AI methods will provide further potential for process improvements.

Acknowledgments

The authors are grateful to Michael Schrattbauer for contributions with respect to the contents of the present paper.

References

1. Adams. Version v2021.0.1. Retrieved July 13, 2025, from https://hexagon.com/products/product-groups/computer-aided-engineering-software/adams.
2. Ferhadbegović, B. (2008). *Development and application of a transient tire model for the vehicle dynamics simulation of agricultural tractors* (in German), [Doctoral dissertation, Institut für Agrartechnik], Shaker Verlag Aachen.
3. Freund, R.W., & Hoppe, R.W. (2007). *Stoer/Bulirsch: Numerical Mathematics 1* (in German). Springer.
4. Fuchs, W., Jedinger-Pauschenwein, G., & Holl, H. (2024, September 24–27). *Field path detection for tractors based on acceleration measurements and virtual multibody system simulations* [Conference presentation]. 40th Danubia-Adria Symposium on Advances in Experimental Mechanics, Gdańsk, Poland.

5. Fuchs, W., & Pauschenwein, G. (2019). From field path profile detection to component testing. *ATZheavy duty worldwide*, *12*(2), 50–55. https://doi.org/10.1007/s41321-019-0022-x

6. FTire. Version 2021-1. Retrieved July 13, 2025, from https://www.cosin.eu.

7. Gattringer, O. (2023). *Virtual road for loads in concept phase using MBS and FEMFAT LAB, engineer vehicle dynamics analysis* [Conference presentation]. Magna ECS Simulation Conference, Linz.

8. Gipser, M. (2007). FTire – the tire simulation model for all applications related to vehicle dynamics. *Vehicle System Dynamics*, *45*(sup1), 139–151. https://doi.org/10.1080/00423110801899960

9. Jedinger-Pauschenwein, G., Fuchs, W., & Holl, H. (2024, September 24–27). *Virtual load case definition for off-road vehicles: Methodology based on multibody system simulation* [Conference presentation]. 40th Danubia-Adria Symposium on Advances in Experimental Mechanics, Gdańsk, Poland.

10. Leister, G. (2009). *Tire and chassis development: strategy, methods, tools, and applications* (in German). ATZ-MTZ Fachbuch, Vieweg und Teubner.

11. Oertel, C. (2007). *Tire modeling in full vehicle simulation: from real-time models to load spectrum analysis* (in German). Haus der Technik.

12. Popp, K., & Schiehlen, W. (2010). *Ground vehicle dynamics*. Springer.

13. Reichl, S. (2011). *Inverse dynamics and trajectory tracking of underactuated multibody systems* [Doctoral dissertation, Vienna University of Technology].

14. Renius, K.T. (2020). *Fundamentals of tractor design*. Springer.

15. Schiller, S. (2018). *Tractor global loading, method optimization* [Master's thesis, University of Applied Sciences]. Upper Austria.

16. Schrattbauer, M. (2024). *Field path profile detection for tractors* [Unpublished master's thesis, Johannes Kepler University]. Linz, Austria.

17. Shabana, A.A. (2013). *Dynamics of multibody systems* (4th ed.). Cambridge University Press.

18. Wiesebrock, A. (2016). *A generic road surface model for vehicle dynamics simulation* (in German). Springer Fachmedien Wiesbaden.

19. Witteveen, W. (2023). *Iterative method for the coupling of arbitrarily many spatially distributed simulations and/or test rigs to a dynamic overall system* [Conference presentation]. Magna ECS Simulation Conference, Linz, Austria.

Manuscript received December 31, 2024; accepted for publication March 31, 2025; published online July 15, 2025.